Journal of Materials Chemistry B

Accepted Manuscript

This article can be cited before page numbers have been issued, to do this please use: L. Shi, Y. Wang, Z. Chu, Y. Yin, D. Jiang, J. Luo, S. Ding and W. Jin, *J. Mater. Chem. B*, 2016, DOI: 10.1039/C6TB02658C.

ROYAL SOCIETY OF CHEMISTRY

rsc.li/materials-b

View Article Online
DOI: 10.1039/C6TB02658C

Table of Contents

Highly sensitive and reusable electrochemical mercury biosensor based on tunable vertical single-walled carbon nanotubes and a target recycling strategy

Lei Shi, Yan Wang, Zhenyu Chu, Yu Yin, Danfeng Jiang, Jingyi Luo, Shiming Ding* and Wanqin Jin*

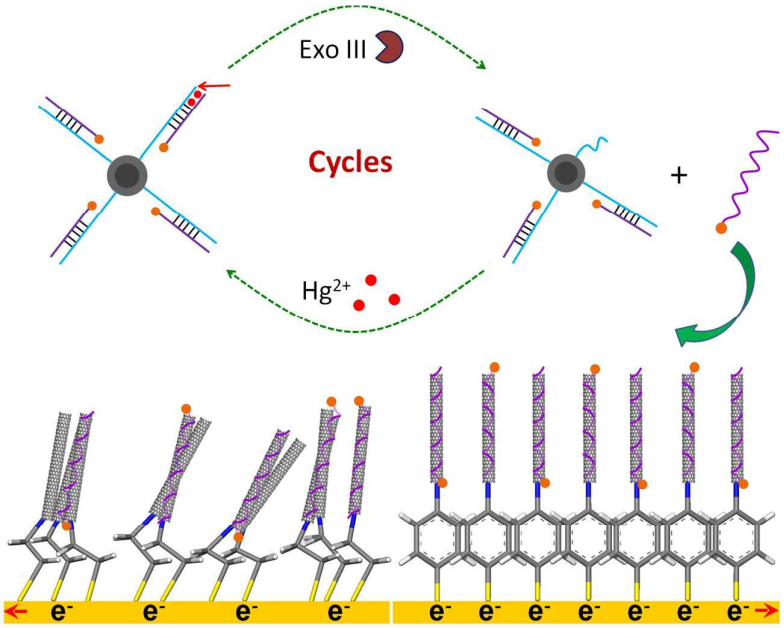

Conformational regulation of SAMs was proposed for controllable growth of v-SWCNTs, which were served to construct a high-performance mercury biosensor with a target recycling strategy.

View Article Online
DOI: 10.1039/C6TB02658C

Journal Name

ARTICLE

Highly sensitive and reusable electrochemical mercury biosensor based on tunable vertical single-walled carbon nanotubes and a target recycling strategy

Received 00th January 20xx,
Accepted 00th January 20xx

DOI: 10.1039/x0xx00000x

www.rsc.org/

Lei Shi,[a] Yan Wang,[a] Zhenyu Chu,[b] Yu Yin,[c] Danfeng Jiang,[b] Jingyi Luo,[b] Shiming Ding*[a] and Wanqin Jin*[b]

In this work, a novel electrochemical Hg^{2+} biosensor was presented with a high sensitivity and excellent reusability. The sensor was based on tunable vertical single-walled carbon nanotubes (v-SWCNTs) and a target recycling strategy. A facile and scalable approach involving the conformational regulation of self-assembled monolayers was established for the fabrication of v-SWCNTs with tailored orientation and homogeneity. The obtained v-SWCNTs possessed superior properties including a large specific area, high electrical conductivity, and excellent substrate binding strength, opening up a wide horizon for advanced electrochemical applications. Meanwhile, an efficient Hg^{2+} recycling strategy was designed using exonuclease III. In this strategy, a trace amount of Hg^{2+} triggered consecutive nicking reactions, and numerous report probes were released to bind with v-SWCNTs through π-π interactions. Based on the innovative design, an ultralow detection limit of 3 fM (S/N = 3), a wide linear range from 10 fM to 1 μM, a high selectivity, and a good reliability were achieved for an Hg^{2+} assay in water and serum samples using the prepared biosensor. Besides, due to the reversibility of π-π interactions, the stable v-SWCNTs interface was regenerated for 50 consecutive measurements without obvious signal loss, making it a promising candidate in routine and efficient Hg^{2+} monitoring.

Introduction

Mercury ions (Hg^{2+}) are highly toxic heavy metal ions that represent a severe hazard to the environment and human health even at low concentrations.[1] Much effort has focused on developing effective methods for Hg^{2+} detection, including atomic absorption/emission spectroscopy,[2] inductively coupled plasma mass spectrometry,[3] fluorescent and colorimetric techniques,[4-8] and electrochemical methods.[9, 10] Among these techniques, electrochemical approaches are particularly advantageous because of their high sensitivity, low cost, and simple operation. Besides, thymine-thymine (T-T) mismatches in DNA are known to bind with Hg^{2+} in aqueous solutions, forming unique DNA duplexes with stable T-Hg^{2+}-T pairings.[11] These interactions provide an opportunity for selective Hg^{2+} detection. Therefore, the integration of electrochemistry and biology offers a new route towards Hg^{2+} detection with a high sensitivity and selectivity.[12, 13]

For successful electrochemical biosensing schemes, effective signal amplification strategies are crucial for improving the performance of low-level detection. One frequently used strategy is to develop various electrode materials.[14-16] Single-walled carbon nanotubes (SWCNTs) have been widely used for electrode preparation because of their unique physicochemical properties.[17-19] Vertically aligned SWCNTs (v-SWCNTs) are particularly appealing for use in electroanalytical applications, because these structures increase the number of available binding sites for analytes, allow these molecules to easily access the electrode surface, and facilitate electron transfer at sensing interfaces.[20-22] Although chemical vapor deposition (CVD) is particularly efficient for preparing v-SWCNTs, it is expensive and technically demanding.[23] Besides, a versatile press-transfer technology has been reported for constructing various carbon-based films.[24, 25] However, it is difficult to effectively realize vertical SWCNT growth because of the requirement of a filtration step.[26] Recently, an attractive chemical assembly technique is introduced for fabricating v-SWCNTs,[27, 28] due to its simplicity, reliability and high compatibility with mass production. In spite of these advantages, it remains a great challenge to achieve well-oriented and homogeneous v-SWCNTs using this method, due to that SWCNTs spontaneously attach and easily bundle on self-assembled monolayers (SAMs). To the best of our knowledge, these morphological parameters of v-SWCNTs are closely associated with their electronic and interfacial properties.[29, 30] Nevertheless, few efforts have been dedicated to the construction of v-SWCNTs with desired morphologies using the chemical assembly. Therefore,

[a] State Key Laboratory of Lake Science and Environment, Nanjing Institute of Geography and Limnology, Chinese Academy of Sciences, Nanjing 210008, P. R. China. E-mail: smding@niglas.ac.cn. Tel: +86-25-86882207. Fax: +86-25-86882207.
[b] State Key Laboratory of Materials-Oriented Chemical Engineering, College of Chemical Engineering, Nanjing Tech University, Nanjing 210009, P. R. China. E-mail: wqjin@njtech.edu.cn. Tel: +86-25-83172266. Fax: +86-25-83172292.
[c] School of Environmental and Chemical Engineering, Jiangsu University of Science and Technology, Zhenjiang 212003, P. R. China.
Electronic Supplementary Information (ESI) available: See DOI: 10.1039/x0xx00000x

View Article Online DOI: 10.1039/C6TB02586G

developing facile and reliable approaches to prepare v-SWCNTs with tailored orientation and homogeneity is of critical importance for high-performance electrochemical applications.

Target recycling is another powerful strategy for signal amplification,[31] in which various nucleases, including endonucleases and exonucleases, allow the direct recycling and reuse of targets. This reuse leads in-turn to a substantial signal amplification.[32, 33] To overcome a common limitation caused by the requirement of a specific recognition sequence for nicking endonucleases,[34, 35] exonuclease III (Exo III) is used because it does not require a specific recognition sequence.[36-38] Recently, it is discovered that the nicking reaction towards DNA duplexes with metal ion-mediated base pairing (e.g., T-Hg^{2+}-T) can also be realized with Exo III.[39] This attractive property provides an opportunity to design promising Hg^{2+} recycling strategy and realize sensitive Hg^{2+} assay.

In this work, a facile and scalable approach was demonstrated for the controllable preparation of v-SWCNTs using the chemical assembly, in which the conformational regulation of SAMs was used to control the orientation and homogeneity of v-SWCNTs. The prepared v-SWCNTs had significantly enhanced properties, making them a promising platform for electrochemical applications. Meanwhile, a novel Exo III-assisted Hg^{2+} recycling strategy was designed, in which consecutive nicking reactions occurred in the presence of trace amounts of Hg^{2+} and led to an increase in the release of report probes. The released report probes bound with the v-SWCNTs through reversible π-π interactions and acted as effective indicators of Hg^{2+} concentrations. Using this measurement design, a novel electrochemical Hg^{2+} biosensor was constructed, and a high-performance assay was created for femtomolar levels of Hg^{2+} with a satisfactory reusability.

Experimental

Materials and reagents

All oligonucleotides were synthesized by TaKaRa Biotechnology Co., Ltd. (Dalian, China), including the assistant probe (A-probe): 5'-NH_2-$(CH_2)_6$-GCT AAG CCA TAG ATC AAT GCG CGG GAC TGT CTT T-3' and the report probe (R-probe): 3'-Methylene blue-ACG GGT ATC TAG TTA CGC GCC CTG TCT GTT T-5'. SWCNT (purity>95%), 4-aminothiophenol, 2-aminoethanethiol, ethylenediamine, 1,4-benzendiamine, sodium dodecyl sulfate (SDS), tris(hydroxymethyl)aminomethane (Tris-base), 1-ethyl-(3-3'-dimethylaminopropyl) carbodiimide (EDC), dimethyl sulfoxide (DMSO), Nhydroxysuccinimide (NHS) and 2-(N-morpholino)ethanesulfonic acid (MES) were purchased from Sigma-Aldrich. Exo III was obtained from New England Biolabs. Carboxylic acid-modified magnetic beads (MBs, 300 nm in diameter) were obtained from Allrun Nanoscience & Technology Co., Ltd. (Shanghai, China). Other chemicals were of analytical grade, and triple-distilled water was used throughout.

Thickness measurements and density functional theory (DFT) simulations of SAMs

Ellipsometry measurements were used to calculate the thicknesses of the SAMs, which were performed using the 632.8 nm line of a He/Ne laser at an incidence angle of 70°. Ellipsometric angles (Δ and Ψ) were determined for both clean and SAM-modified substrates. Thickness calculations were based on a three-phase ambient atmosphere/SAMs/gold model.[40] The DafIBM program (Rudolph Technologies) was used to calculate thicknesses, assuming that the refractive indexes of 2-aminoethanethiol and 4-aminothiophenol SAMs were 1.48 and 1.65, respectively. The final thicknesses of the SAMs were obtained by taking the average of three sampling points.

DFT simulations were introduced to optimize conformations of SAMs[41, 42] and details are described in the ESI†.

Controllable fabrication of v-SWCNTs on conductive substrates

Gold substrate was prepared by sputtering a 100 nm thick gold top layer onto the quartz wafer, and was immersed in an ethanol solution containing 2-aminoethanethiol or 4-aminothiophenol (0.5 mM) to form various SAMs. SAMs of 2-aminoethanethiol and 4-aminothiophenol were referred to here as S-SAM and R-SAM, respectively. SWCNTs were chemically shortened following an established procedure,[22] and resuspended in DMSO by sonicating. Subsequently, the gold substrates modified with SAMs were vertically dipped into the solution containing the SWCNTs for 8 h, and coupling agents of EDC and NHS were added to promote the condensation reaction between $–NH_2$ groups of the SAMs and –COOH groups of the SWCNTs to form amide bonds. The v-SWCNTs fabricated on S-SAM and R-SAM were referred to v-SWCNTs(S) and v-SWCNTs(R), respectively.

To explore the scalability of proposed approach, glass carbon substrates were introduced to fabricate v-SWCNTs with a similar procedure, in which two other molecules of ethylenediamine and 1,4-benzendiamine were selected to form various SAMs on substrates by amine cation radical formation.[43] $–NH_2$ groups at two terminals were used to interact with the carbon substrates and bind with –COOH groups on SWCNTs respectively.

Immobilization of A-probes on MBs to prepare A-probe/MBs

A-probes were attached to MBs using an amide-coupling reaction.[44] Briefly, 300 μL carboxylated MBs (5 mg/mL) was rinsed twice with 300 μL MES buffer (25 mM, 0.1 M NaCl, pH 7.5). A-probes (5 nM) in 200 μL MES buffer were added to the washed MBs and incubated for 30 min at room temperature under gentle shaking. Subsequently, 5 μL EDC (10 mg/mL) and 5 μL NHS (15 mg/mL) were added to the suspension containing MBs and A-probes, and 90 μL MES buffer was added to reach a final volume of 300 μL. This mixture was incubated for 3 h at 4 °C. The resulting A-probe/MBs were incubated with Tris-HCl buffer (20 mM, 0.2 M NaCl, pH 7.5) for 15 min to quench unreacted –COOH groups. The collected A-probe/MBs were thoroughly washed, resuspended in 1 mL Tris buffer, and stored at 4 °C.

View Article Online
DOI: 10.1039/C6TB02658C

Construction of v-SWCNT-based electrochemical biosensor for Hg^{2+} detection

In a typical experiment, R-probes (10 nM) in 20 µL hybridization buffer (10 mM Tris-HCl, 1 mM EDTA, 0.2 M NaCl, pH 7.5) were added into 100 µL A-probe/MBs, and 80 µL hybridization buffer was then added to reach a final volume of 200 µL. The resulting mixture was then incubated for 2 h at 37 °C under gentle shaking. Afterwards, the solution was magnetically separated to remove excess R-probes, and the hybridized A-probe/MBs were resuspended in 200 µL Tris-HCl buffer. Small aliquots (5 µL) of solutions containing various Hg^{2+} concentrations were added into 50 µL hybridized A-probe/MB solution, and the mixtures were incubated under gentle shaking for 0.5 h. Subsequently, 10 units (U) of Exo III were injected, and the nicking reaction proceeded at 37 °C for 0.5 h. Finally, the resulting mixture was magnetically separated, and v-SWCNTs modified substrates were incubated in the clear solution for 2 h, following by thoroughly washed with Tris-HCl buffer before electrochemical measurements.

Electrochemical measurements

All electrochemical measurements were performed with a CHI 660E electrochemical workstation (Shanghai Chenhua, China). A three-electrode system was used consisting of a v-SWCNTs working electrode, a platinum auxiliary electrode, and an Ag/AgCl (saturated KCl) reference electrode. Cyclic voltammetry (CV) was performed at a scan rate of 100 mV/s, and square wave voltammetry (SWV) was performed with a potential step size of 4 mV, an amplitude of 25 mV, and a frequency of 5 Hz.

Standard deviation of five replicate tests was designated as the error bar in each data point. Relative standard deviation (RSD) was also calculated to ensure the reliability of measurements and maximum RSD (m-RSD) in each curve was presented in the work.

Results and discussion

Characterization of v-SWCNTs(S) and v-SWCNTs(R)

In addition to acting as binding agents, SAMs have recently been shown to control the growth of functional hybrid films, in which different molecular conformations and terminal functionalities induce the oriented attachment of appropriate growth species.[42, 45] Inspired by this significant discovery, we hypothesize that v-SWCNTs with desired morphologies could be created by regulating the conformations of SAMs. Accordingly, two functional molecules were chosen to produce different SAMs on gold substrates through the Au-S bond, which was confirmed with the x-ray photoelectron spectroscopy (XPS). As shown in Fig. S1, binding energies (BEs) at ca. 84, 164, 285 and 399 eV are attributed to Au4f, S2p, C1s and N1s species respectively, and the BE in N1s spectrum at 399.4 eV is ascribed to the terminal amine groups.[46]

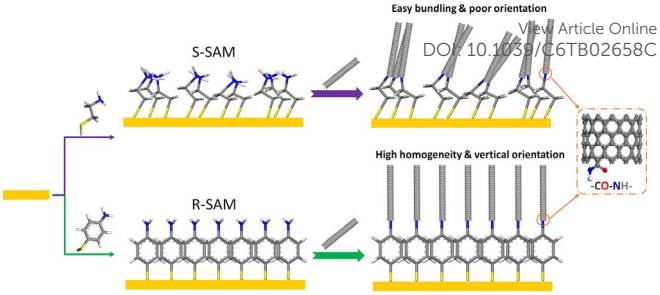

Fig. 1 Fabrication scheme for the vertical growth of SWCNTs on gold substrates modified with S-SAM and R-SAM.

On account of the softness of the alkyl chains and the potential interaction between $–NH_2$ and gold atoms,[47] the soft molecules in S-SAM would bend on the gold surface, and the $–NH_2$ groups of adjacent molecules may approach each other due to the hydrogen bond.[48] In contrast, rigid molecules in R-SAM would uprightly anchor on the gold surface, and $–NH_2$ groups may evenly distribute because of the confined motions of benzene rings. To further explore these interactions, ellipsometry measurement as well as DFT simulation was introduced. Ellipsometry is an effective method to measure the thickness of SAMs, and it is revealed that the average thicknesses of S-SAM and R-SAM were 2.1 Å ± 0.4 Å and 5.9 Å ± 0.3 Å respectively. As the physical lengths of the corresponding molecules are ca. 4.1 Å and 6.4 Å, it can be deduced that a flexible and disordered S-SAM while a relatively erect R-SAM were formed on the gold surfaces. Besides, similar results were also observed from the DFT simulations (Fig. S2).

Subsequently, different SAM-modified substrates were introduced for the growth of v-SWCNTs through the formation of amide bond (shown in Fig. 1). This interaction was confirmed in the N1s spectrum with a BE at ca. 400.2 eV, which belongs to the NH–C=O (Fig. S3). As expected, S-SAM had fewer available binding sites and did not provide a powerful structural direction for the growth of v-SWCNTs(S) due to its disordered and flexible structure. This resulted in the formation of only local domains with v-SWCNTs (Fig. 2A). Agglomerated $–NH_2$ groups also caused the bundling of SWCNTs, and bundles with large width were observed, as shown in Fig. 2B. Since the AFM tip used has a typical radius of curvature near 10 nm, the actual dimensions of the v-SWCNTs were estimated after deconvolution of the AFM data based on a simple geometric consideration. Therefore, v-SWCNTs(S) with a dominant height of ~40 nm and width of ~30 nm were obtained (Fig. 2C). In contrast, v-SWCNTs(R) were uniformly and consecutively formed on a substrate modified with R-SAM (Fig. 2D), and the bundles were less wide (Fig. 2E). These features resulted from the enhanced directing force and evenly distributed $–NH_2$ groups of the R-SAM. Accordingly, the v-SWCNTs(R) had an improved height of ~60 nm and a narrower width of ~10 nm (Fig. 2F). These results indicate that the conformational regulation of SAMs is feasible and effective

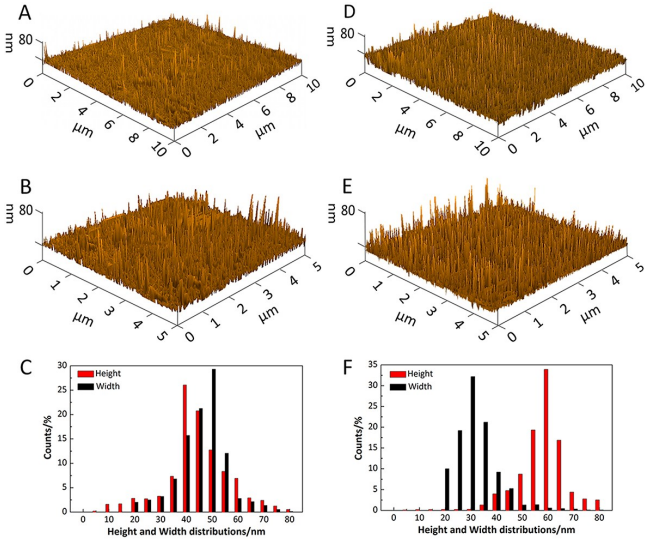

Fig. 2 (A) and (B) AFM images of v-SWCNTs(S) at low and high magnifications. (C) Histograms of the height and width distributions of v-SWCNTs(S). (D) and (E) AFM images of v-SWCNTs(R) at low and high magnifications. (F) Histograms of the height and width distributions of v-SWCNTs(R).

to regulate the growth of v-SWCNTs with controllable orientation and homogeneity. Besides, these spikes in AFM images were further investigated by Raman spectroscopy (Fig. S4). There are two strong bands around 1590 cm^{-1} (G-band) and 190 cm^{-1} (radial breathing mode, RBM), and a weak band at 1350 cm^{-1} (D-band). The presence of RBM is unique to SWCNTs.[49] Furthermore, the scalability of proposed approach was investigated, and ethylenediamine (soft backbone) and 1,4-benzendiamine (rigid backbone) molecules owned comparable molecular structures with those of 2-aminoethanethiol and 4-aminothiophenol were used. As suggested in Fig. S5, the BEs in N1s spectra at about 398.9 and 399.4 eV belong to the N–C the –NH– respectively, revealing that these functional molecules were successfully grafted on the substrates. As a result, v-SWCNTs with analogous morphologies were obtained. It is demonstrated that this approach was suitable for more relevant molecules, and had great potential to prepare desirable v-SWCNTs on various substrates.

CV measurements were performed to evaluate the electrochemical properties and binding stabilities of the fabricated v-SWCNTs on gold substrates. As shown in Fig. 3A, compared to the low oxidation peak current of 6.9 μA on the substrate, increased peak currents from 21.8 μA for v-SWCNTs(S) to 31.7 μA for v-SWCNTs(R) were obtained, indicating that the vertical structures created a larger electroactive surface area. Meanwhile, the peak potential differences (ΔE_p) decreased from 74.0 mV for the substrate to 66.9 mV for v-SWCNTs(S) and 55.9 mV for v-SWCNTs(R). These decreases in ΔE_p were accompanied by increased peak currents (Fig. S6). As a lower ΔE_p value indicates a more rapid electron transport rate, the highly vertical and homogenous v-SWCNTs(R) possess both an

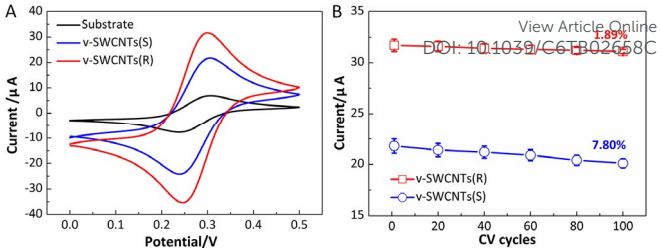

Fig. 3 (A) CV curves generated at the substrate, v-SWCNTs(S), and v-SWCNTs(R) in 1 mM $K_3Fe(CN)_6$ containing 0.1 M KCl. (B) Peak currents recorded during 100 consecutive CV measurements using v-SWCNTs(S) (m-RSD of 3.12%) and v-SWCNTs(R) (m-RSD of 1.90%).

enhanced specific area and an improved electrical conductivity compared to those of the v-SWCNTs(S). To assess the binding stabilities of the v-SWCNTs on the substrates, the prepared v-SWCNTs were scanned for 100 consecutive cycles, and the oxidation peak currents were recorded. As shown in Fig. 3B, only a subtle current decrease of 1.89% was obtained for v-SWCNTs(R), while a larger decrease of 7.80% was observed for v-SWCNTs(S). The R-SAM with an upright structure and highly distributed $–NH_2$ groups facilitated more chemical interactions with SWCNTs than did the S-SAM. These interactions resulted in the enhanced binding strength of the v-SWCNTs(R) on the substrates.

Meanwhile, the density of v-SWCNTs(R) was easily adjusted by changing the surface coverages of the R-SAMs via the incubation time in 4-aminothiophenol. As shown in Fig. 4, more SWCNTs were vertically and homogenously anchored on substrates at higher R-SAM coverages, because additional binding sites were available for the interaction with SWCNTs. It should also be noted that the chemically shortened SWCNTs had various lengths, and the shorter SWCNTs preferentially interacted with the R-SAM than the longer ones did, due to their faster adsorption dynamics.[27] Consequently, an increased height of the v-SWCNTs(R) was observed at a higher R-SAM coverage.

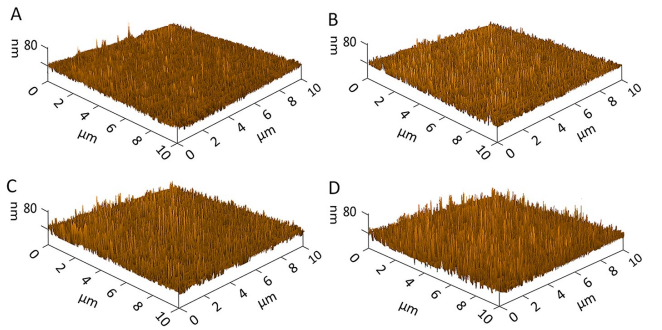

Fig. 4 AFM images of v-SWCNTs(R) on R-SAMs incubated in 4-aminothiophenol for different time of (A) 2 h, (B) 4 h, (C) 6 h, and (D) 8 h.

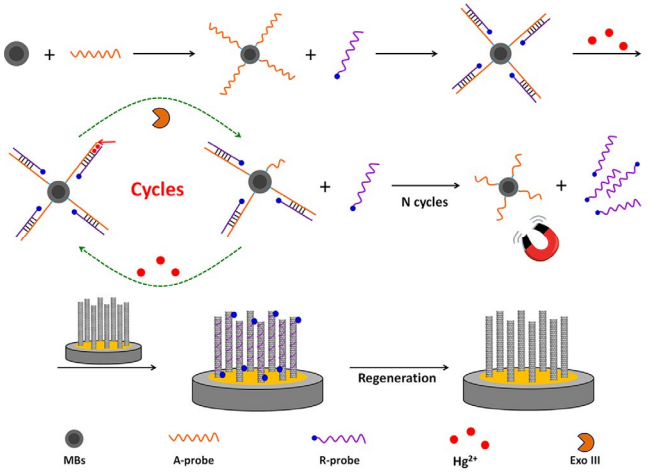

Fig. 5 Design of an Exo III-assisted sensing scheme for Hg^{2+} detection based on v-SWCNTs.

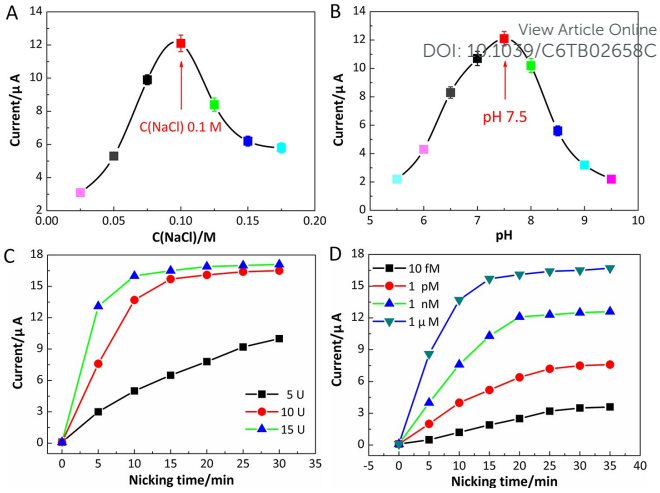

Fig. 6 Optimization of (A) NaCl concentration (m-RSD of 6.41%) and (B) pH (m-RSD of 5.76%) for the detection of 1 nM Hg^{2+}. Effect of (C) Exo III units in 1 μM Hg^{2+} and (D) Hg^{2+} concentrations in 10 U Exo III on sensor responses over time.

Additional CV measurements were performed to explore the electrochemical properties of the v-SWCNTs(R) prepared at different coverages of R-SAMs. CV curves were recorded at R-SAM-modified substrates, as shown in Fig. S7. Compared with that obtained at a bare substrate, the oxidation peak currents at the R-SAM-modified substrates gradually reduced as ΔE_p increased, indicating that the R-SAMs decreased the active electrode area and hindered electron transfer reactions, especially at higher coverages. After v-SWCNTs(R) were grown on the R-SAMs, the peak currents increased significantly, while ΔE_p decreased with a maximum at the incubation time of 6 h (Fig. S8). The specific surface area was limited when there was a low density of v-SWCNTs(R). However, a surface crowded with v-SWCNTs, which was prepared at a high R-SAM coverage, decreased the rate of electron transfer and impeded the diffusion of biomolecules and the transmission of signals. Therefore, the optimal incubation time of 6 h was selected for the R-SAM in order to fabricate v-SWCNTs(R) with a large surface area and rapid electron transfer.

The above results confirm that the prepared v-SWCNTs(R), which had highly vertical and homogenous structures and controllable surface densities, possessed significantly enhanced surface area, fast electron transport rate, and excellent binding strength on substrates. These merits make the v-SWCNTs(R) a promising platform for the construction of novel and high-performance electrochemical Hg^{2+} biosensors.

Hg^{2+} detection scheme based on the prepared v-SWCNTs

As depicted in Fig. 5, A-probes were covalently attached to MBs via the amide bond, which was demonstrated in the XPS spectra (Fig. S9). The BEs in N1s spectrum at about 397.9, 399.4 and 400.2 eV are attributed to the =N–, –NH– and NH–C=O. The NH–C=O confirms the effective immobilization of A-probes on MBs. The P2p band with a BE at ca. 131 eV and the presence of =N– and –NH– stem from phosphate groups and bases in A-probes respectively. R-probes with methylene blue tags were hybridized to the A-probes through partial base pairing, leaving free T-T pairs at their terminal ends for Hg^{2+} recognition. In the presence of Hg^{2+}, free T bases on the A-probes and R-probes become tightly coupled through the formation of stable T-Hg^{2+}-T, leading to the generation of nicking sites for Exo III. When Exo III was added, the nicking reaction was initiated, and sequences of A-probes were cut into mononucleotides, resulting in the dissociation of R-probes from the MBs' surfaces. Subsequently, Hg^{2+} was simultaneously dissociated and became available for the formation of more T-Hg^{2+}-T structures. This triggered the next nicking cycle. As a result, many R-probes were released into the solution per Hg^{2+} target. These R-probes then adsorbed to the v-SWCNTs through π-π interactions, and the resulting signal was used to measure Hg^{2+} concentration. The presence of P2p band and additional =N– in N1s spectrum confirms the binding of R-probes on the SWCNTs (Fig. S10). Besides, the reversibility of these π-π interactions endowed a potential reusability of the v-SWCNTs.

Electrochemical investigations of the Hg^{2+} biosensor

Due to its excellent resolution of the electrochemical signals in similar sensing systems,[35, 50] SWV was introduced to monitor the responses of the Hg^{2+} biosensor. The feasibility of the sensing scheme was first validated, as shown in Fig. S11A. In contrast to the low signal (1.6 μA) measured in the absence of Hg^{2+}, a significantly enhanced response (10.8 μA, ca. 7-fold) was observed at a low concentration of 0.1 nM Hg^{2+}, indicating that the proposed sensing scheme was feasible for Hg^{2+} assay. By sonicating the R-probes attached v-SWCNTs(R) in Britton-Robinson buffer solution containing 0.5% SDS for 5 min,[51] the response from the R-probes was eliminated (ca. 1.9 μA, Fig. S11B). This indicates that the R-probes were effectively removed from the v-SWCNTs through this simple regeneration procedure, ensuring the reusability of the prepared sensing platform.

Additional optimizations of the experimental conditions were also implemented. Ionic strength is known to strongly influence the immobilization of A-probes and their subsequent hybridization with R-probes.[52] As shown in Fig. 6A, when the NaCl concentration increased from 0.025 M to 0.1 M, more A-probes were immobilized on the MBs because of reduced electrostatic repulsion, and the response signals gradually increased. However, the additional A-probes produced at excessively high NaCl concentrations severely hindered hybridization with R-probes and the recognition of Hg^{2+}. This resulted in significantly decreased signals. Therefore, 0.1 M NaCl was used in subsequent experiments for the immobilization of A-probes on MBs. Since the hybridization of A-probes and R-probes was accelerated at high NaCl concentrations, 0.2 M NaCl was selected in the hybridization process (Fig. S12).

The effect of pH on sensor response was also determined, because pH was important for the sensitivity of a biosensor. As shown in Fig. 6B, the response signals enhanced as the pH was increased from 5.5 to 7.5, but then decreased at pH values from 7.5 to 9.5. The highest sensitivity was observed at pH 7.5, possibly because T became quaternized at low pH values and Hg^{2+} precipitates formed at high pH values.[53]

Since Hg^{2+} can alter the biological activity of Exo III, different units of Exo III were tested. As shown in Fig. 6C, a low unit of Exo III (5 U) was insufficient to digest the hybridized DNA and resulted in low signals even at long nicking time. In contrast, 10 U Exo III promoted a high nicking efficiency, and signals reached saturation levels within 15 min. However, excessive Exo III (15 U) caused the nicking efficiency to increase instead of the saturation value. Therefore, 10 U Exo III was chose for subsequent Hg^{2+} assays.

Nicking time was also optimized to improve sensor sensitivity (Fig. 6D). As anticipated, the nicking reaction was extremely rapid and the signals plateaued within 15 min at 1 μM Hg^{2+}, indicating that Exo III cleaved approximately 100% of A-probes in this time. The nicking rate reduced when the Hg^{2+} concentration was gradually decreased. Even so, relatively short nicking time of 30 min was required at a low Hg^{2+} concentration of 10 fM. The nicking efficiency reported here was considerably higher than those reported previously.[37, 54] The possible reason was ascribed to that well-dispersed MBs modified with DNA strands in homogenous solution could facilitate the formation of T-Hg^{2+}-T structures and the processing of nicking reaction. As a result, a nicking time of 30 min was used in subsequent tests.

Performance of the electrochemical Hg^{2+} biosensor

The sensitivity of the biosensor was further investigated by varying the Hg^{2+} concentrations. As shown in Fig. 7A, the response signals enhanced with increasing Hg^{2+} concentrations from 0 fM to 1 μM, because additional R-probes were released. A linear relationship was obtained between signal change (Δi) and the logarithm of Hg^{2+} concentration from 10 fM to 1 μM with a regression equation of $\Delta i = 22.64 + 1.46\mathrm{Log}(C_{Hg^{2+}})$ (R^2 = 0.994). An ultralow detection limit of 3 fM (S/N = 3) was

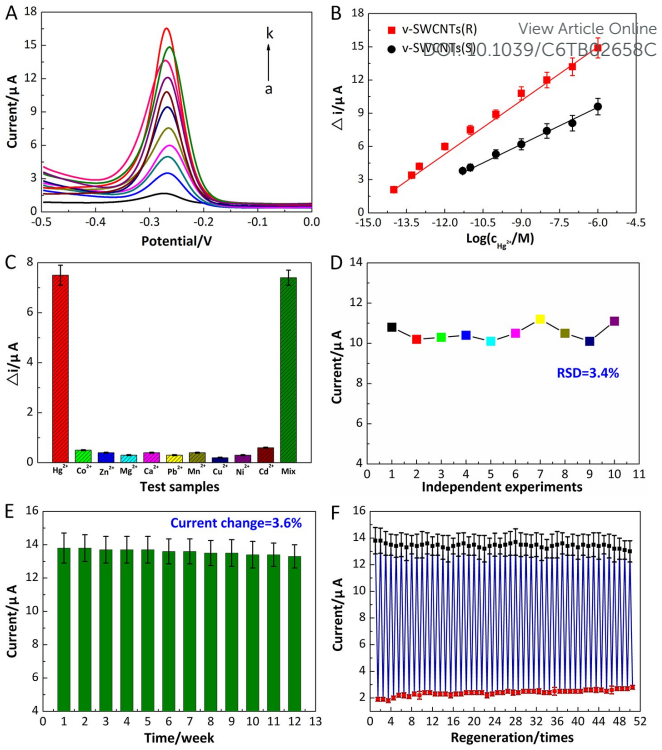

Fig. 7 (A) SWV responses of the biosensor at different Hg^{2+} concentrations (a to k correspond to 0 fM, 10 fM, 50 fM, 0.1 pM, 1 pM, 10 pM, 0.1 nM, 1 nM, 10 nM, 0.1 μM and 1 μM respectively). (B) Calibration curves of Δi *vs*. logarithm of Hg^{2+} concentration. (C) Selectivity (m-RSD of 5.26%) of the biosensor. (D) Reproducibility of the biosensor in 0.1 nM Hg^{2+}. (E) Stability (m-RSD of 6.43%) and (F) reusability (m-RSD of 6.78%) of the biosensor in 10 nM Hg^{2+}.

achieved (Fig. 7B), and the m-RSD in calibration curve was 5.91%, guaranteeing the high precision of the biosensor. This wide linear range over 8 orders of magnitude in Hg^{2+} concentrations was mainly due to the high binding capacity of T for Hg^{2+} in the homogenous reaction system. Although more assay time was consumed than some other T-Hg^{2+}-T based electrochemical biosensors, the performance of the prepared biosensor was superior to that of most reported ones (shown in Table S1).[12, 13, 35, 55-60] The performance of an Hg^{2+} biosensor based on v-SWCNTs(S) was also investigated for comparison. As shown in Fig. 7B, Δi of the v-SWCNTs(S)-based sensor was lower than that of the v-SWCNTs(R)-based sensor, and a relatively high detection limit of 2 pM (S/N = 3) was observed for this biosensor. Clearly, the homogenous v-SWCNTs(R) with a large specific surface area effectively bound with more R-probes than v-SWCNTs(S), which was favorable for the signal acquisition. Meanwhile, the high electrical conductivity of the v-SWCNTs(R) facilitated signal transmission. These merits contributed to the significantly enhanced response signals, resulting in a high-performance Hg^{2+} assay using the v-SWCNTs(R)-based biosensor.

The selectivity of the biosensor was determined by monitoring Δi with other common divalent metal cations, e.g. Co^{2+}, Zn^{2+}, Mg^{2+}, Ca^{2+}, Pb^{2+}, Mn^{2+}, Cu^{2+}, Ni^{2+}, and Cd^{2+}. The solutions tested included 10 pM Hg^{2+}, 1 mM of each metal ion, and a mixture of the two. As shown in Fig. 7C, the biosensor

exhibited negligible responses to 1 mM of the other metal ions compared to its response to 10 pM Hg^{2+}. The biosensor was highly selective for Hg^{2+} because of the specific interactions of Hg^{2+} and T for the formation of T-Hg^{2+}-T.

Since reproducibility is extremely important for establishing reliable and practical assays, independent experiments were tested and response signals were recorded. As shown in Fig. 7D, subtle signal variations were observed with an RSD of 3.40%, indicating that an excellent reproducibility was obtained with the prepared biosensors. In addition, a batch of freshly prepared biosensors was stored at 4 °C for 1 to 12 weeks to test their stability. These biosensors' responses decreased slightly over time, and a signal change of 3.60% was observed after 12 weeks (Fig. 7E), revealing that the prepared biosensors were satisfactorily stable. Furthermore, because of the reversible interactions between R-probes and v-SWCNTs(R), reusability was tested after consecutive regeneration treatments. The response recovered nearly to its initial value, and the v-SWCNTs(R) sensing interface could be reused for 50 times without a significant loss in signal (Fig. 7F). This superior reusability was mainly attributed to the high binding strength of the prepared v-SWCNTs(R) on the substrate.

Practical applications of the Hg^{2+} biosensor

Because of its excellent sensitivity and selectivity, the prepared biosensor was next used for Hg^{2+} assays in lake water and human serum samples. To allow the biosensor to be compared with ICP-MS, lake water samples were first treated with UV digestion and acidification to liberate Hg^{2+} from other species. Results from the biosensor were compared to those from ICP-MS, as listed in Table S2. As no Hg^{2+} was present in the human serum, the standard addition method was used and the results were provided in Table S3. Hg^{2+} concentrations determined with our biosensor were in good agreement with those measured using ICP-MS or known from the standard additions. The recovery and RSD were satisfactory. These results indicate that the prepared biosensor is capable and reliable for Hg^{2+} detection in real samples.

Conclusions

In this work, a highly sensitive and reusable electrochemical Hg^{2+} biosensor was constructed. Two major innovations in this work included: (i) the conformational regulation of SAMs was shown to enable the controllable growth of v-SWCNTs with desired orientation and homogeneity. These morphological features provided the v-SWCNTs with significantly enhanced properties. (ii) An efficient Hg^{2+} recycling strategy (assisted by Exo III) was designed, in which numerous R-probes were released when only trace amounts of Hg^{2+} was present. These R-probes subsequently bound with the v-SWCNTs for the highly efficient Hg^{2+} assay. It is anticipated that v-SWCNTs prepared in this work would find great potential in multiple advanced applications in electronic and energy-related systems, and the designed target recycling strategy could be extended to a broad range of sensing applications.

Acknowledgements

View Article Online
DOI: 10.1039/C6TB02658C

This work was supported by the National Natural Science Foundation of China (Nos. 41322011, 41571465, 21607159), the Natural Science Foundation of Jiangsu Province (No. BK20161087), National High-level Personnel of Special Support Program and Nanjing Institute of Geography and Limnology, CAS (NIGLAS2015QD07).

Notes and references

1. L. Cui, J. Wu and H. Ju, *Biosens. Bioelectron.*, 2015, **63**, 276.
2. H. Erxleben and J. Ruzicka, *Anal. Chem.*, 2005, **77**, 5124.
3. G. M. M. Rahman, M. M. Wolle, T. Fahrenholz, H. M. S. Kingston and M. Pamuku, *Anal. Chem.*, 2014, **86**, 6130.
4. H. N. Kim, W. X. Ren, J. S. Kim and J. Yoon, *Chem. Soc. Rev.*, 2012, **41**, 3210.
5. M. Xu, Z. Gao, Q. Wei, G. Chen and D. Tang, *Biosens. Bioelectron.*, 2016, **79**, 411.
6. V. Sharma, A. K. Saini and S. M. Mobin, *J. Mater. Chem. B*, 2016, **4**, 2466.
7. Z. S. Wu, M. K. Feng, X. X. Chen and X. J. Tang, *J. Mater. Chem. B*, 2016, **4**, 2086.
8. Y. Tao, Y. H. Lin, Z. Z. Huang, J. S. Ren and X. G. Qu, *Talanta*, 2012, **88**, 290.
9. J. Wang, J. M. Lu, S. B. Hocevar, P. A. M. Farias and B. Ogorevc, *Anal. Chem.*, 2000, **72**, 3218.
10. X.-Z. Yao, Z. Guo, Q.-H. Yuan, Z.-G. Liu, J.-H. Liu and X.-J. Huang, *ACS Appl. Mater. Interfaces*, 2014, **6**, 12203.
11. Y. Miyake, H. Togashi, M. Tashiro, H. Yamaguchi, S. Oda, M. Kudo, Y. Tanaka, Y. Kondo, R. Sawa, T. Fujimoto, T. Machinami and A. Ono, *J. Am. Chem. Soc.*, 2006, **128**, 2172.
12. R.-M. Kong, X.-B. Zhang, L.-L. Zhang, X.-Y. Jin, S.-Y. Huan, G.-L. Shen and R.-Q. Yu, *Chem. Commun.*, 2009, 5633.
13. C. Tortolini, P. Bollella, M. L. Antonelli, R. Antiochia, F. Mazzei and G. Favero, *Biosens. Bioelectron.*, 2015, **67**, 524.
14. C. N. LaFratta and D. R. Walt, *Chem. Rev.*, 2008, **108**, 614.
15. L. Shi, Z. Chu, Y. Liu, W. Jin and X. Chen, *Biosens. Bioelectron.*, 2013, **49**, 184.
16. L. Shi, Z. Chu, Y. Liu, W. Jin and N. Xu, *Adv. Funct. Mater.*, 2014, **24**, 7032.
17. S. M. Taghdisi, N. M. Danesh, A. S. Emrani, M. Ramezani and K. Abnous, *Biosens. Bioelectron.*, 2015, **73**, 245.
18. D. Vilela, A. Anson-Casaos, M. T. Martinez, M. C. Gonzalez and A. Escarpa, *Lab Chip*, 2012, **12**, 2006.
19. J. X. Wang, M. X. Li, Z. J. Shi, N. Q. Li and Z. N. Gu, *Anal. Chem.*, 2002, **74**, 1993.
20. J. J. Gooding, R. Wibowo, J. Q. Liu, W. R. Yang, D. Losic, S. Orbons, F. J. Mearns, J. G. Shapter and D. B. Hibbert, *J. Am. Chem. Soc.*, 2003, **125**, 9006.
21. F. Patolsky, Y. Weizmann and I. Willner, *Angew. Chem. Int. Ed.*, 2004, **43**, 2113.
22. F. J. Rawson, C. L. Yeung, S. K. Jackson and P. M. Mendes, *Nano Lett.*, 2013, **13**, 1.
23. S. Maruyama, E. Einarsson, Y. Murakami and T. Edamura, *Chem. Phys. Lett.*, 2005, **403**, 320.
24. A. Martin, L. Vazquez and A. Escarpa, *J. Mater. Chem. A*, 2016, **4**, 13142.
25. F. Della Pelle, L. Vázquez, M. Del Carlo, M. Sergi, D. Compagnone and A. Escarpa, *Chem. Eur. J.*, 2016, **22**, 12761.

26. D. Vilela, J. Garoz, A. Colina, M. C. Gonzalez and A. Escarpa, *Anal. Chem.*, 2012, **84**, 10838.
27. Z. F. Liu, Z. Y. Shen, T. Zhu, S. F. Hou, L. Z. Ying, Z. J. Shi and Z. N. Gu, *Langmuir*, 2000, **16**, 3569.
28. P. Diao and Z. Liu, *Adv. Mater.*, 2010, **22**, 1430.
29. P. Diao and Z. F. Liu, *J. Phys. Chem. B*, 2005, **109**, 20906.
30. S. J. Kang, C. Kocabas, T. Ozel, M. Shim, N. Pimparkar, M. A. Alam, S. V. Rotkin and J. A. Rogers, *Nat. Nanotechnol.*, 2007, **2**, 230.
31. Y. Guo, J. Wu and H. Ju, *Chem. Sci.*, 2015, **6**, 4318.
32. L. Bai, Y. Chai, X. Pu and R. Yuan, *Nanoscale*, 2014, **6**, 2902.
33. P. Tong, L. Zhang, J. J. Xu and H. Y. Chen, *Biosens. Bioelectron.*, 2011, **29**, 97.
34. Q. Wang, C. Yang, Y. Xiang, R. Yuan and Y. Chai, *Biosens. Bioelectron.*, 2014, **55**, 266.
35. L. Shi, Z. Chu, Y. Liu, W. Jin and X. Chen, *Biosens. Bioelectron.*, 2014, **54**, 165.
36. C. Gao, X. Y. Yu, S. Q. Xiong, J. H. Liu and X. J. Huang, *Anal. Chem.*, 2013, **85**, 2673.
37. C. Chen, J. Zhao, J. Jiang and R. Yu, *Talanta*, 2012, **101**, 357.
38. Z. X. Zhou, W. Wei, Y. J. Zhang and S. Q. Liu, *J. Mater. Chem. B*, 2013, **1**, 2851.
39. F. Xuan, X. Luo and I. M. Hsing, *Anal. Chem.*, 2013, **85**, 4586.
40. D. K. Jacquelin, M. A. Perez, E. M. Euti, N. Arisnabarreta, F. P. Cometto, P. Paredes-Olivera and E. M. Patrito, *Langmuir*, 2016, **32**, 947.
41. M. Gliboff, H. Li, K. M. Knesting, A. J. Giordano, D. Nordlund, G. T. Seidler, J.-L. Bredas, S. R. Marder and D. S. Ginger, *J. Phys. Chem. C*, 2013, **117**, 15139.
42. L. Shi, Z. Chu, X. Dong, W. Jin and E. Dempsey, *Nanoscale*, 2013, **5**, 10219.
43. J. Y. Liu, L. Cheng, B. F. Li and S. J. Dong, *Langmuir*, 2000, **16**, 7471.
44. H. Nie, Z. Yang, S. Huang, Z. Wu, H. Wang, R. Yu and J. Jiang, *Small*, 2012, **8**, 1407.
45. C. Scherb, A. Schoedel and T. Bein, *Angew. Chem. Int. Ed.*, 2008, **47**, 5777.
46. D. Wan, S. J. Yuan, G. L. Li, K. G. Neoh and E. T. Kang, *ACS Appl. Mater. Interfaces*, 2010, **2**, 3083.
47. A. H. Pakiari and Z. Jamshidi, *J. Phys. Chem. A*, 2007, **111**, 4391.
48. S. Mukherjee, S. Majumdar and D. Bhattacharyya, *J. Phys. Chem. B*, 2005, **109**, 10484.
49. M. S. Dresselhaus, G. Dresselhaus, A. Jorio, A. G. Souza and R. Saito, *Carbon*, 2002, **40**, 2043.
50. L. Shi, Z. Chu, Y. Liu and W. Jin, *J. Mater. Chem. B*, 2015, **3**, 3134.
51. X. Z. Zhang, K. Jiao, S. F. Liu and Y. W. Hu, *Anal. Chem.*, 2009, **81**, 6006.
52. A. W. Peterson, R. J. Heaton and R. M. Georgiadis, *Nucleic Acids Res.*, 2001, **29**, 5163.
53. N. Wang, M. Lin, H. Dai and H. Ma, *Biosens. Bioelectron.*, 2016, **79**, 320.
54. C. Luo, H. Tang, W. Cheng, L. Yan, D. Zhang, H. Ju and S. Ding, *Biosens. Bioelectron.*, 2013, **48**, 132.
55. J. Chen, J. Tang, J. Zhou, L. Zhang, G. Chen and D. Tang, *Anal. Chim. Acta*, 2014, **810**, 10.
56. Y. Zhang, H. Zhao, Z. Wu, Y. Xue, X. Zhang, Y. He, X. Li and Z. Yuan, *Biosens. Bioelectron.*, 2013, **48**, 180.
57. Z. Zhang, J. Yin, Z. Wu and R. Yu, *Anal. Chim. Acta*, 2013, **762**, 47.
58. C. Mei, D. Lin, C. Fan, A. Liu, S. Wang and J. Wang, *Biosens. Bioelectron.*, 2016, **80**, 105.
59. G. V. Guerreiro, A. J. Zaitouna and R. Y. Lai, *Anal. Chim. Acta*, 2014, **810**, 79.
60. R. Tian, X. Chen, N. Jiang, N. Hao, L. Xu and C. Yao, *J. Mater. Chem. B*, 2015, **3**, 4805.

View Article Online DOI: 10.1039/C6TB02658C